Electrochemical behaviour of low temperature grown iron fluoride thin films

Yoshinari Makimura, Aline Rougier, Lydia Laffont, Manfred Womes, Jean-Claude Jumas, Jean-Bernard Leriche, J.-M. Tarascon

Electrochemical behaviour of low temperature grown iron fluoride thin films

Y. Makimura [a], A. Rougier [a,*], L. Laffont [a], M. Womes [b], J.-C. Jumas [b], J.-B. Leriche [a], J.-M. Tarascon [a]

[a] *Laboratoire de Réactivité et de Chimie des Solides, CNRS UMR-6007, Université de Picardie Jules Verne, 33 rue Saint Leu, 80039 Amiens Cedex, France*
[b] *Laboratoire des Agrégats Moléculaires et Matériaux Inorganiques, CNRS UMR-5072, Université Montpellier II, Place E. Bataillon, 34095 Montpellier Cedex 5, France*

Abstract

By coupling a homemade substrate holder with a refrigerated ethanol cryogenic system, we succeeded in growing thin films by Pulsed Laser Deposition at substrate temperatures as low as −50 °C. The benefit of enlarging substrate temperatures to negative values is illustrated through the example of iron fluoride thin films, for which the substrate temperature is a key factor governing the FeF_2 or/and FeF_3 phase deposition. Using a FeF_3 target, the X-ray diffraction study shows that the "FeF_x" thin films grown at 600 °C correspond to a single well-crystallized FeF_2 phase (S.G.: $P4_2/mnm$) as opposed to a mixture of FeF_3 and FeF_2 phases for room temperature substrate, and a single FeF_3 phase (S.G.: $R\bar{3}c$) having quite an intense (0 1 2) Bragg peak at low temperature substrate (−50 °C). Such assignments were confirmed by complementary HRTEM and Mössbauer measurements with the exception of the −50 °C grown film that was shown to contain amorphous FeF_2 together with crystallized FeF_3 phases. The electrochemical behaviour of the FeF_x thin films, namely their voltage profiles, was found to be dependent on the substrate grown temperature.

Keywords: Iron fluorides; Thin film; Pulsed laser deposition; Lithium-ion battery; Low temperature substrate; ^{57}Fe Mössbauer data

1. Introduction

In recent years, nano-sized transition-metal oxides have received an extensive interest regarding their use as electrode materials in lithium-ion batteries [1]. Such interest has recently been amplified with the arrival of Li-driven conversion reactions leading to M–O based electrodes with outstanding capacity gains over classical insertion electrodes. These reactions, which are taking advantage of electrochemistry at the nano-scale, have been extended to other classes of materials such as binary metal sulphides, nitrides, phosphides and fluorides [2–8]. Indeed transition-metal fluorides, which as iron-based compounds are attractive in terms of their non-toxicity and cost [6,7], present the advantage of having a high ionic character, leading to high operating voltages compared to oxides in lithium cells. However owing to their insulator character, iron fluorides suffer from poor kinetics. Focusing on bulk material, Amatucci et al. reported improved properties for carbon metal fluorides nano-composites electrodes (e.g. having a 20 nm crystallite size) cycled at 75 °C. Another interesting alternative consists in their thin film preparation preventing any binder or electronic conductor addition. The number of papers reporting the growth of Fe-based fluoride thin films is rather low, and more importantly none of them deals with their electrochemical characterization in lithium cells [9–14]. In our group, thin films of several families of materials, among them oxides, phosphides, metal, hydrides, have been successfully grown using the Pulsed Laser Deposition technique [15–17]. Indeed, the versatility of the PLD technique provides unique advantages to tune thin films

* Corresponding author. Tel.: +33 3 22 82 76 04; fax: +33 3 22 82 75 90.
E-mail address: aline.rougier@sc.u-picardie.fr (A. Rougier).

properties by playing with the deposition conditions (target nature, pressure, laser energy, etc.). However, to our knowledge the growth of thin films at substrate temperatures below zero has never been reported. Herein, we embark on the first study reporting deposition at low temperature, namely −50 °C, of iron fluoride thin films used as positive electrode in lithium batteries.

2. Experimental

Iron fluoride thin films were grown on stainless steel substrates from high purity FeF_3 target under vacuum (5.0×10^{-5} Pa) by pulsed laser deposition using a KrF excimer laser (Lambda Physik, Compex 102, $\lambda = 248$ nm). To prevent the iron fluoride thin films from any air exposure upon handling and characterization, the PLD system was equipped with a glove box [17]. The classical configuration means a laser energy of 180 mJ, a frequency of 2 or 10 Hz and 1 h duration, the substrate temperature varies from RT to 600 °C. To achieve low substrate temperature depositions, we designed a specific substrate holder, cooled through metallic tubes by refrigerated ethanol flowing from a cryogenic device equipped with a regulator of temperature (Vasse Julabo FP50). Substrate temperatures as low as −50 °C were successfully achieved by decreasing the laser energy to 120 mJ as a 180 mJ energy produces heat inside the chamber limiting the inside temperature to −20 °C.

Thin films were characterized by X-ray diffraction using an X-ray diffractometer (Philips PW 1729) with Cu Kα radiation. TEM and HRTEM imaging were performed using a FEI TECNAI F20 S-TWIN equipped with an EDX analysis detector. The film deposition was achieved directly on copper grids coated with a lacy carbon film. The diffraction patterns were performed using the Selected Area Electron Diffraction (SAED) mode. The SAED patterns obtained on polycrystalline samples were analyzed using the process diffraction software [18].

Conversion Electron Mössbauer Spectroscopy (CEMS) was carried out at room temperature in the constant acceleration mode, using equipment from Wissel and Ortec. ^{57}Co(Rh) with a nominal activity of 10 mCi was used as a source. The velocity scale was calibrated by means of a room temperature CEMS spectrum of α-Fe, which was also used as the reference for all isomer shifts. The hyperfine parameters Isomer Shift (δ) and Quadrupole Splitting (ΔE_q) were determined by fitting Lorentzian lines to the experimental data, making use of the ISO fit program [19].

The electrochemical behaviour of iron fluoride thin films deposited on stainless steel substrates, and used as positive electrode, was characterized using standard 2035-size coin cells. The negative electrode, a lithium foil was separated from the positive electrode by GF/D borosilicate glass fibre sheet, soaked with 1 M $LiPF_6$ dissolved in ethylene carbonate (EC)/dimethyl carbonate (DMC) solution (1/1 by volume) electrolyte. The cells were assembled in a glove box filled with argon. Electrochemical measurements were carried out galvanostatically at a current density of $0.56\ \mu A \cdot cm^{-2}$ (voltage profiles) and of $2.82\ \mu A \cdot cm^{-2}$ (cycling tests) in a voltage window of 3.60–0.05 V using a Macpile controller.

3. Results and discussion

For a 600 °C substrate temperature, the XRD profile of iron fluoride thin film deposited from a FeF_3 target corresponds to the well-crystallized tetragonal FeF_2 phase (S.G.: $P4_2/mnm$) (Fig. 1). The signature of the FeF_3 phase, represented by the single (0 1 2) peak (S.G.: $R\bar{3}c$ [20]), starts to appear with decreasing the substrate temperature (⩽400 °C [21]) and becomes clearly visible for a RT substrate. Despite the single peak existence, the FeF_3 phase identification is unambiguous as other FeF_3 phases, namely the pyrochlore-type structure [22], the HTB-type structure $FeF_3(H_2O)_{0.33}$ [23], do not show any XRD peaks at a similar two theta position. For a RT substrate, the sharpness of the (0 1 2) FeF_3 peak is opposed to the broadness of the (1 1 0) FeF_2 one, indicating higher crystallinity for the FeF_3 phase compared to the FeF_2 one. Using the Scherrer formula, average crystallite sizes of 39 and 15 nm were calculated for FeF_3 and FeF_2 phases, respectively. First attempts to isolate the FeF_3 phase by decreasing the laser energy, increasing the deposition rate, and increasing the fluorine content inside the target (mixture of XeF_2/FeF_3 target) remained unsuccessful. On the contrary, thanks to our own homemade low temperature set up, we observed a progressive and full disappearance of the (1 1 0) FeF_2 XRD peak with decreasing the temperature. Finally for a substrate temperature as low as −50 °C, the (0 1 2) FeF_3 peak remained as a single peak suggesting, at first sight, the sole existence of the FeF_3 phase.

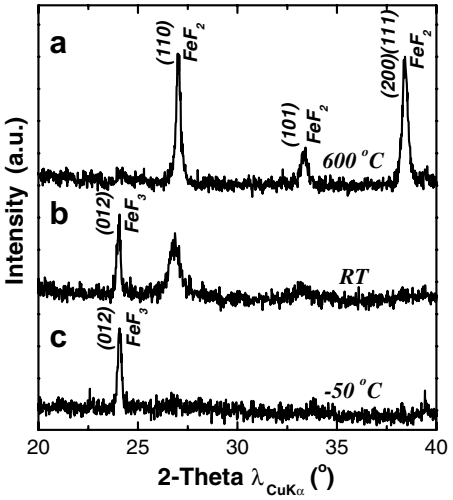

Fig. 1. X-ray diffraction patterns of iron fluoride thin films deposited on stainless steel substrates from FeF_3 target under vacuum of 5.0×10^{-5} Pa at several substrate temperatures, i.e., 600 (a), RT (b) and −50 °C (c), for 1 h at a repetition rate of 10 Hz. Miller indexes were given by assuming a tetragonal lattice of FeF_2 (space group: $P4_2/mnm$) and a rhombohedral lattice of FeF_3 (space group: $R\bar{3}c$) in hexagonal setting.

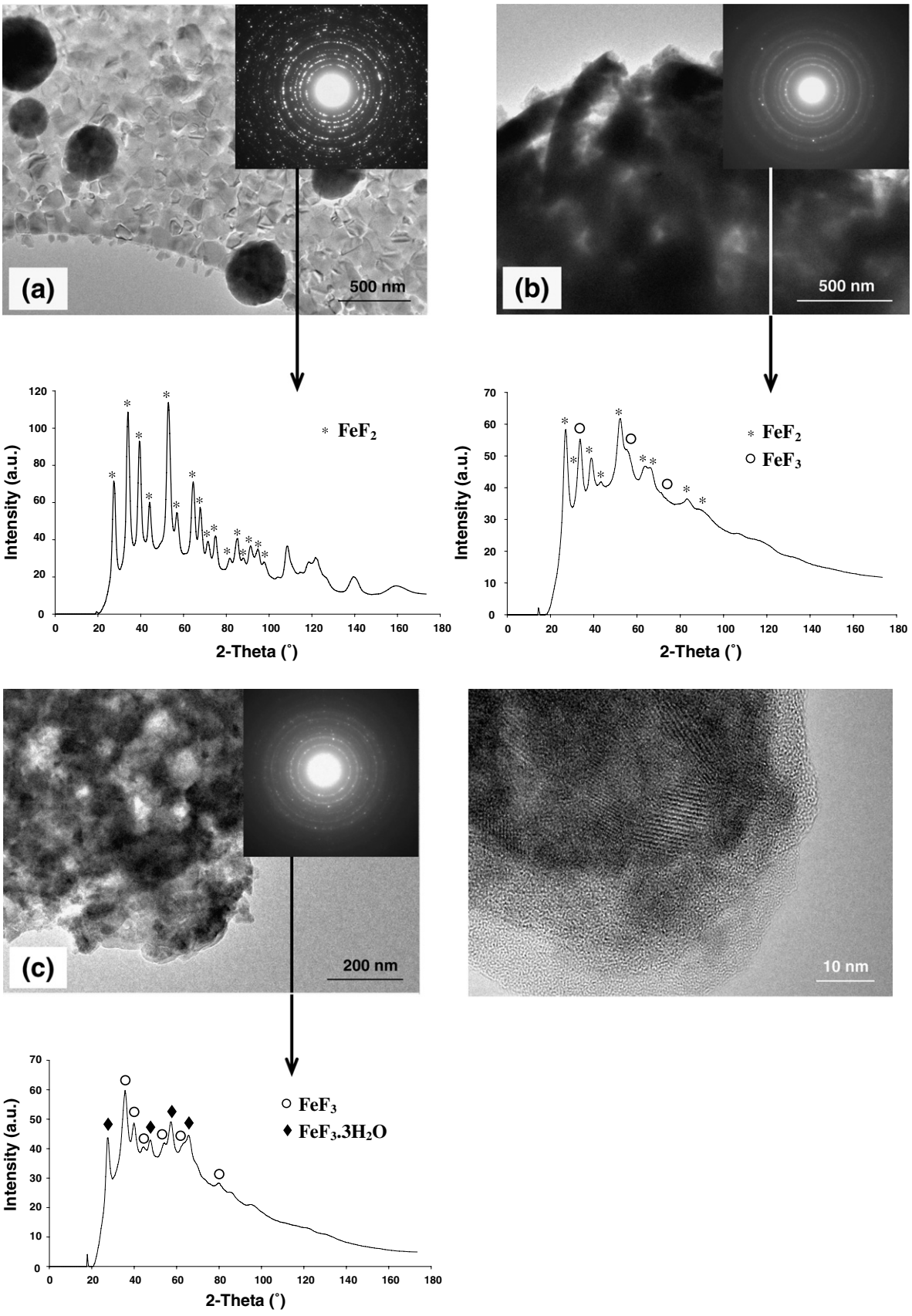

Fig. 2. HRTEM and SAED micrographs of iron fluoride thin films deposited on stainless steel substrates from FeF_3 target under vacuum of 5.0×10^{-5} Pa at several substrate temperatures, i.e., 600 (a) , RT (b) and −50 °C (c), for 1 h at a repetition rate of 2 Hz. Using the process diffraction software, the SAED pattern is transformed to a pseudo powder diffraction pattern (Intensity $= f(2\theta)$, λ CuK_α) in order to have a precise determination of the phase.

The bright field image of the film deposited at 600 °C is composed of particles of 50–200 nm size with dispersed droplets (100–400 nm size) (Fig. 2a). The XRD-like diagram corresponding to the SAED pattern clearly shows that the film is FeF_2 and is very well-crystallized. On the contrary, the droplets are amorphous. The film deposited at room temperature is still composed of crystallized particles of about 50–200 nm but the line profile of the corresponding SAED pattern indicates the coexistence of the FeF_2 phase together with FeF_3 (Fig. 2b). For the film grown at −50 °C (Fig. 2c), the bright field image shows the existence of an amorphous layer localized around the 20–50 nm crystallized nanoparticles. As deduced from the SAED pattern of the bright field image, crystallized domains correspond to the FeF_3 phase with a proportion of hydrate FeF_3. The presence of $FeF_3 \cdot H_2O$ probably results from the reaction to moisture of the LT FeF_3 film, when stored in the glove box, and should not be attributed to the deposition step, which is besides performed in high vacuum (10^{-5} Pa). If the HRTEM observations are well consistent with the XRD data for the films deposited above RT, the nature of the co-existing amorphous phase detected for the film deposited at −50 °C remains undetermined.

To further examine the stable phase of iron fluoride thin film in terms of electronic structures, CEMS was carried out. CEMS spectra indicated that the iron fluoride thin film deposited at 600 °C was a single phase of FeF_2 (Fig. 3, Table 1), which hyperfine parameters ($\delta = 1.35$ mm/s, $\Delta E_q = 2.78$ mm/s) are comparable to previous values ($\delta = 1.34$ mm/s, $\Delta E_q = 2.76$ mm/s) [24], in agreement with XRD data shown in Fig. 1. Although the XRD pattern of the thin film deposited at −50 °C corresponds to the FeF_3 phase, CEMS spectra indicate a more complex situation enlisting a mixture of iron (III) fluoride (47%) and iron (II) fluoride (53%). The hyperfine parameters of such iron (II) fluoride ($\delta = 1.28$ mm/s, $\Delta E_q = 2.45$ mm/s), close to those of crystallized FeF_2, and the line width broadening ($\Gamma = 0.54$ mm/s) clearly give evidence of the development of an amorphous FeF_2 phase. Concerning the iron (III) fluoride, the hyperfine parameters ($\delta = 0.50$ mm/s, $\Delta E_q = 0.52$ mm/s) by comparison with amorphous FeF_3 ($\delta = 0.45$ mm/s, $\Delta E_q = 0.55$ mm/s) [25] and the lack of magnetic hyperfine field are in agreement with the formation of poorly crystallized FeF_3. This occurrence of superparamagnetic effects at room temperature for FeF_3 can be explained by the size of grains (10–20 nm) and the thickness of grain boundaries as previously discussed for nanostructured iron fluoride powders [26,27]. These results suggest that the iron fluoride thin film deposited at −50 °C was a two-phase mixture of poorly-crystallized FeF_3 and amorphous FeF_2. Thin film deposition performed at low substrate temperature and under extreme vacuum conditions (10^{-5} Pa) was found to be amorphous FeF_2 rather than FeF_3 as expected owing to fluorine volatility.

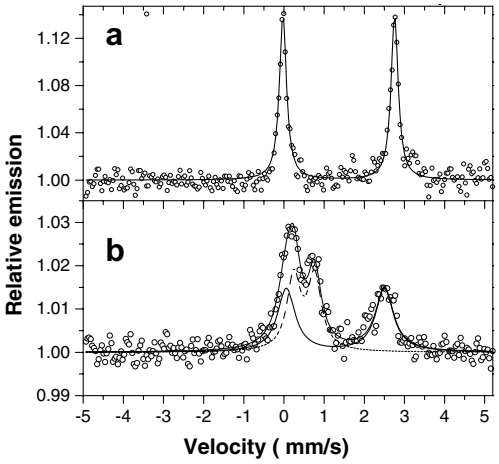

Fig. 3. ^{57}Fe CEMS spectra of iron fluoride thin films grown from FeF_3 target at 600 (a) and −50 °C (b).

At this point it is important to describe the electrochemical performances of such films with respect to Li. A rough estimation of the capacity for the 600 °C film, converted in number of lithium inserted and extracted, was calculated from the film thickness considering 80% of the density of the bulk FeF_2 (4.28 g · cm^{-3}), i.e. 3.42 g · cm^{-3}. For the −50 °C film, based on the Mössbauer estimation, the calculation was done assuming a 50% FeF_2 + 50% FeF_3 film composition and 80% of the bulk density (3.96 g · cm^{-3}), i.e., 3.17 g · cm^{-3}. However, caution has to be applied here not to overinterpret the data, since the exact film composition is not well determined. The galvanostatic cycling of lithium cells with iron fluoride thin films deposited at 600 and −50 °C as positive electrodes (Fig. 4) exhibit similar trends when cycled between 3.60 and 0.05 V, namely: (1) a large polarization (nearly 1 V) between charges and discharges, (2) a large irreversible capacity on the first cycle owing to a charge capacity being nearly half of the discharge capacity, and (3) a sustained capacity retention

Table 1
^{57}Fe hyperfine parameters of iron fluoride thin films grown from FeF_3 target at 600 and −50 °C

Films	δ (mm/s)	ΔE_q (mm/s)	2Γ (mm/s)	C (%)	Attribution
FeF_3 target (600 °C)	1.37 (1)	2.78 (1)	0.22 (1)	100	FeF_2
FeF_3 target (−50 °C)	1.28 (2)	2.45 (3)	0.54 (4)	53	Amorph. FeF_2
	0.50 (1)	0.52 (2)	0.41 (3)	47	FeF_3

The various parameters are: δ = Isomer Shift relative to α-Fe, ΔE_q = Quadrupole Splitting, 2Γ = Line Width at Half Maximum, C = contribution of subspectra to the spectrum.

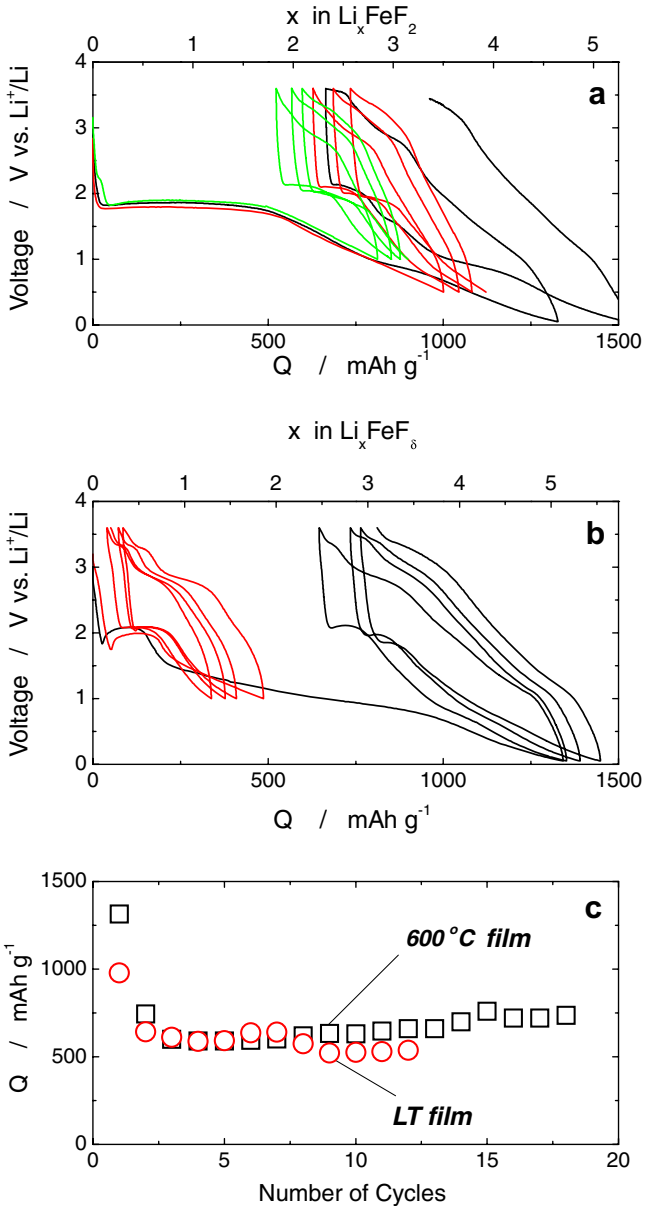

Fig. 4. Discharge and charge curves of lithium cells using iron fluoride thin films as positive electrode. Films were deposited on stainless steel substrates from FeF_3 target under vacuum of 5.0×10^{-5} Pa at several substrate temperatures, i.e., 600 (a) and −50 °C (b). The cells were tested in various voltage windows 3.6 to 1.0, 0.5 and 0.05 V at a current density of 1 μA/1.77 cm^2 (0.56 μA · cm^{-2}) (a,b), and 5 μA/1.77 cm^2 (2.8 μA · cm^{-2}) (c) at 25 °C. The electrolyte used was 1 M $LiPF_6$ dissolved in EC / DMC solution (1/1 by volume). (c) Corresponding capacity versus the number of cycles curves.

upon cycling as shown in Fig. 4c. Nevertheless, the voltage traces are quite different for both films. For the 600 °C film (Fig. 4a), the first discharge profile shows first the appearance of a plateau at 1.90 V having a 2 Li amplitude, followed by a continuous voltage decay down to 0.05 V corresponding to an extra storage capacity of 2.5 Li per unit formula. This plateau remains well pronounced upon cycling as long as the discharge cut-off voltage remains greater than 0.50 V. The −50 °C grown film (Fig. 4b) behaves quite differently as the first discharge curve shows first a plateau near 2.20 V having an amplitude of solely 0.8 Li as opposed to 2 previously, followed by two different voltage sloping ranges going from 2.20 to 1.00 V and from 1.00 to 0.05 V, and corresponding to Li capacities of 2 and 1.5, respectively. As previously, the first plateau remains upon cycling as long as the discharge cut-off voltage is limited to 1 V, but progressively diminishes to disappear after 10 cycles (Fig. 4b) when lowering the discharge cut-off voltage to 0.05 V.

At this point a legitimate question arises as to whether the Li reactivity mechanism reported for the FeF_2 and FeF_3 powders prevails as we move to thin films. Amatucci's group [7,8] deduced from bulk powder characterizations that the overall lithium uptake and removal in fluorides occurs through the conversion process, $nLi + MX_m \rightarrow M + LiX_{m/n}$, leading therefore to an expected 2 Li per Fe for the complete reduction of FeF_2. In contrast, the reduction mechanism was shown to be different for FeF_3 since it first enlists the insertion of Li into FeF_3 leading to a Li_xFeF_3 phase; the latter was then undergoing a conversion process resulting in the formation of Fe nanoparticles embedded into a LiF matrix, and which were converting back to the FeF_2 phases upon subsequent charges. The discharge plateau, which total capacity extends up to 2 lithiums, observed during the reduction of $Li/FeF_{2(600\ °C\ thin\ film)}$ cells is strongly indicative that our films react towards Li like the powders; that is to say according to the following conversion reaction ($FeF_2 + 2Li^+ + 2e^- \rightleftarrows 2LiF + Fe$). Such conversion mechanism has been confirmed by HRTEM measurements that have shown the coexistence of both crystallized Fe and LiF phases together with an amorphous layer at the end of the first discharge, and the partial conversion back to FeF_2 upon recharge.

A similar comparison between FeF_3 powders and thin films is at first not as straightforward, since upon discharge, $Li/FeF_{3(powders)}$ cells have shown a 3 V pseudo plateau corresponding to the insertion of nearly 0.9 Li into FeF_3, while no capacity is observed at such voltage for $Li/FeF_{3(-50\ °C\ thin\ film)}$ cell. This came as a surprise, since the 3 V insertion reaction was shown to have fast kinetics capable of sustaining numerous cycles at C rate. In contrast, upon discharge of such a cell (Fig. 4b) a decrease in the potential down to 1.90 V is followed by a plateau at 2.20 V, characteristic of a nucleation-growth process at the macroscopic scale. Owing to the same amplitude of this plateau, nearly 0.8 Li^+ per unit formula as the one obtained for FeF_3 powders, it is tempting to speculate that it is also indicative of the Li insertion process into FeF_3. Therefore, why is the potential so different? A possible answer could be rooted in some kinetic limitations as the FeF_3 grown films are carbon-free as opposed to FeF_3 powders composites that contain at least 15% of powders. Interestingly, this improvement with carbon addition is not observed for FeF_2 as there is no potential difference between carbon-free FeF_2 thin films and carbon-containing FeF_2 powder electrodes,

suggesting better kinetics for FeF_2, in agreement with Amatucci's work that shows very little difference in the utilization of FeF_2 powders at room vs. elevated temperatures as compared to FeF_3 powders [28]. We thus believe this potential difference to be the signature of the presence of FeF_3 domains, which are less conductive than the FeF_2 ones. Knowing that the Gibbs free energy of formation for an amorphous phase is higher than that of its crystalline counterpart one could at first explain the slightly highest observed potential (2.2 V instead of 1.9 V) to be nested in the presence of an amorphous FeF_2 phase in our FeF_3 thin films [29,30]. However the fact that we solely observed 0.8 Li at such a voltage rules out this possibility. Finally, the disappearance upon cycling of the 1 bump around 1.90 V is not a surprise as in the conversion reaction the oxidation reaction is incomplete, and we do not convert back to Fe^{3+} but to Fe^{2+}, thus leading to a progressive disappearance of the FeF_3 domains. Therefore, the latter cannot be reduced on the subsequent cycles. Finally after 10 cycles, only FeF_2 is cycling and similar voltage shapes are observed for the 600 and −50 °C films.

Finally, whatever FeF_2 or FeF_3 films, it should be noted that they both show highly reversible extra storage capacities at low potential. Such a low voltage phenomenon is not too surprising as it was reported earlier on in transition-metal oxides, and more recently on transition-metal fluorides. Although such an extra capacity is concomitant with the appearance of a polymeric film resulting from electrolyte degradation, its origin is presently believed to be caused by an interfacial interaction of lithium within the Fe/LiF matrix, possibly leading to a distinct local charging, hence the new concept of interfacial storage as well-known for supercapacitors.

4. Conclusion

For the first time to our knowledge and thanks to a homemade set-up, we report the successful growth of thin films at a substrate temperature as low as −50 °C using the Pulsed Laser Deposition technique. Such achievement was of major importance in the growth of iron fluoride thin films, for which the FeF_3/FeF_2 phase proportion is strongly related to the substrate temperature. Indeed films deposited at 600 °C were a single phase of FeF_2 in a well-crystallized form, whereas films deposited at −50 °C exhibited the XRD pattern corresponding to the FeF_3 phase. However, thanks to HRTEM observations, and more specifically to Mössbauer spectroscopy, the −50 °C deposited film was identified as being a mixture of 47% poorly-crystallized FeF_3 phase and 53% amorphous FeF_2 phase. When tested as positive electrode in lithium cells, voltage profiles of the film deposited at −50 °C were different from the ones grown at 600 °C, corresponding to FeF_2, in an early stage of cycling. After a few cycles, voltage profiles of FeF_x films become similar whatever the deposition temperature. Further understanding of the reaction mechanism of iron fluoride in lithium cells is now in progress in our research group.

Acknowledgement

The authors are thankful the European Network of Excellence ALISTORE (contract No. SES6-CT-2003-503532) that was supporting this work.

References

[1] P. Poizot, S. Laruelle, S. Grugeon, L. Dupont, J.-M. Tarascon, Nature 407 (2000) 496.
[2] F. Gillot, S. Boyanov, L. Dupont, M.L. Doublet, M. Morcrette, L. Monconduit, J-M. Tarascon, Chem. Mater. 17 (2005) 6327.
[3] N. Pereira, M. Balasubramanian, L. Dupont, J. McBreen, L.C. Klein, G.G. Amatucci, J. Electrochem. Soc. 150 (2003) A1118.
[4] J-M. Tarascon, S. Grugeon, M. Morcrette, S. Laruelle, P. Rozier, P. Poizot, C.R. Chim. 8 (2005) 9.
[5] H. Li, G. Richter, J. Maier, Adv. Mater. 15 (2003) 736.
[6] F. Badway, N. Pereira, F. Cosandey, G.G. Amatucci, J. Electrochem. Soc. 150 (2003) A1209.
[7] F. Badway, F. Cosandey, N. Pereira, G.G. Amatucci, J. Electrochem. Soc. 150 (2003) A1318.
[8] B. Bervas, F. Badway, L.C. Klein, G.G. Amatucci, Electrochem. Solid-State Lett. 8 (2005) A179.
[9] H. Ohta, C.A. Ramos, D. Lederman, V. Jaccarino, J. Magn. Magn. Mater. 104–107 (1992) 1741.
[10] D.P. Belanger, M. Lui, R.W. Erwin, Mater. Res. Soc. Symp. Proc. (Magnetic Ultrathin Films) 313 (1993) 755.
[11] J. McChesney, M. Hetzer, H. Shi, T. Charlton, D. Lederman, J. Mater. Res. 16 (2001) 1769.
[12] S.R. Qiu, J.A. Yarmoff, Phys. Rev. B 63 (2001) 115409.
[13] A. Lachter, M. Lascaud, A.S. Barriere, L. Lozano, J. Portier, B. Saboya, J. Crystal Growth 43 (1978) 621.
[14] A.S. Barriere, J.C. Gianduzzo, L. Fournes, Thin Solid Films 89 (1982) 233.
[15] V. Pralong, J.-B. Leriche, B. Beaudoin, E. Naudin, M. Morcrette, J.-M. Tarascon, Solid State Ionics 166 (2004) 295.
[16] I. Bouessay, A. Rougier, P. Poizot, J. Moscovici, A. Michalowicz, J.-M. Tarascon, Electrochim. Acta 50 (2005) 3737.
[17] X. Darok, A. Rougier, V.V. Bhat, L. Aymard, L. Dupont, L. Laffont, J.-M. Tarascon, Thin Solid Films, in press.
[18] J.L. Lábár, Ultramicroscopy 103 (2005) 237.
[19] W. Künding, Nucl. Instrum. Methods 75 (1969) 336.
[20] M. Leblanc, J. Pannetier, G. Ferey, R. De Pape, Rev. Chim. Miner. 22 (1985) 107.
[21] Y. Makimura, A. Rougier, J.-M. Tarascon, Appl. Surf. Sci. 252 (2006) 4587.
[22] R. De Pape, G. Ferey, Mater. Res. Bull. 21 (1986) 971.
[23] M. Leblanc, G. Ferey, P. Chevallier, Y. Calage, R. De Pape, J. Solid State Chem. 47 (1983) 53.
[24] B.S. Yu, H.M. Goff, J. Am. Chem. Soc. 111 (1989) 6558.
[25] M. Eibschütz, M.E. Lines, L.G. Van Uitert, H.J. Guggenheim, G.J. Zydzik, Phys. Rev. B 24 (1981) 2343.
[26] H. Guérault, M. Tamine, J.M. Grenèche, J. Phys.: Condens. Matter. 12 (2000) 9497.
[27] J.M. Grenèche, Hyperfine Interact. 144 (2002) 51.
[28] F. Badway, M. Bervas, N. Pereira, A.N. Mansour, W.-S. Yoon, J. Al-Sharab, I. Plitz, W. Tong, F. Cosandey, G.G. Amatucci, in: Proceedings of the 42nd Power Sources Conference, June 12–15, 2006, Philadelphia, PA, USA.
[29] R-B. Schwarz, W-L. Johnson, Phys. Rev. Lett. 51 (5) (1983) 415.
[30] S-K. Xia, E. Baggio-Saitovich, C. Larica, Phys. Rev. Lett. 49 (2) (1994) 927.